ROBUST MULTISCALE ITERATIVE SOLVERS FOR NONLINEAR FLOWS IN HIGHLY HETEROGENEOUS MEDIA

Y. EFENDIEV, J. GALVIS, S. KI KANG, AND R.D. LAZAROV

Abstract. In this paper, we study robust iterative solvers for finite element systems resulting in approximation of steady-state Richards' equation in porous media with highly heterogeneous conductivity fields. It is known that in such cases the contrast, ratio between the highest and lowest values of the conductivity, can adversely affect the performance of the preconditioners and, consequently, a design of robust preconditioners is important for many practical applications. The proposed iterative solvers consist of two kinds of iterations, outer and inner iterations. Outer iterations are designed to handle nonlinearities by linearizing the equation around the previous solution state. As a result of the linearization, a large-scale linear system needs to be solved. This linear system is solved iteratively (called inner iterations), and since it can have large variations in the coefficients, a robust preconditioner is needed. First, we show that under some assumptions the number of outer iterations is independent of the contrast. Second, based on the recently developed iterative methods (see [15, 17]), we construct a class of preconditioners that yields convergence rate that is independent of the contrast. Thus, the proposed iterative solvers are optimal with respect to the large variation in the physical parameters. Since the same preconditioner can be reused in every outer iteration, this provides an additional computational savings in the overall solution process. Numerical tests are presented to confirm the theoretical results.

1. Introduction

In this paper, we study robust preconditioners for solving finite element approximations of nonlinear flow equations in heterogeneous media. Our motivation stems from Richards' equation ([28]) which describes the infiltration of water into a porous media whose pore space is filled with air and water. In many cases, the heterogeneous porous media is characterized by large variations of the conductivity. For example, in natural porous formations it is common to have several orders of magnitude of variations in the conductivity values. A high contrast, expressed as the ratio between high and low conductivity values, brings an additional scale into the problem. A design of robust preconditioners that converge independent of small scales and high-contrast of the media for nonlinear problems is a challenging task. In this paper, we address this problem for the model of two-phase flow in porous media, the steady-state Richards' equation.

The Richards' equation has the form

$$D_t\theta(u) - \operatorname{div}(k(x,u)\nabla(u+x_3)) = f, \qquad x \in \Omega, \tag{1}$$

where $\theta(u)$ denotes the volumetric fluid content, and $k(x,u) \geq k_0 > 0$ is the relative hydraulic conductivity and k_0 is a constant. We assume that suitable initial and boundary data are provided. The dependence of the volumetric water content and the relative hydraulic conductivity from the pressure head is established experimentally by assuming some functional form. There is a large number of functional forms used by hydrologists and soil scientists. In our numerical experiments, we use three popular among the soil scientists models, namely, Haverkamp, van Genuchten models, and Exponential (see, e.g. [7, 21, 33, 27]).

Date: beginning August 18, 2010, today is: May 21, 2011.
Key words and phrases. FE method, nonlinear permeability, highly heterogeneous media, high contrast media.

In this paper, we are interested in robust preconditioners for the finite element system resulting from the discretization of nonlinear equations when $k(x,u)$ is heterogeneous with respect to space. We consider the steady-state Richards' equation

$$\operatorname{div}(k(x,u)\nabla(u+x_3)) = f, \qquad x \in \Omega, \tag{2}$$

where $k(x,u)$ has high variations in x. In many practical cases, the heterogeneous portion of the relative permeability is given by a spatial field that does not depend on u, i.e., $k(x,u) = k(x)\lambda(u)$. By denoting, $u+x_3$ as a new variable and assuming λ is smooth, we can write the above equation as

$$\operatorname{div}(k(x)\lambda(x,u)\nabla u) = f, \qquad x \in \Omega, \tag{3}$$

where $k(x)$ is a heterogeneous function, while $\lambda(x,u)$ is a smooth function that varies moderately in both x and u. Robust preconditioners for a finite element approximation of Equation (3) with such coefficients will be studied in the paper. We note that coarse-grid approximations of Richards' equation are discussed in literature (e.g., [8, 1, 13]).

Various iterative methods for solving nonlinear equations have been proposed and studied in the past, e.g. [5, 6, 10, 24, 31, 34]. For example, in [5, 31], a nonlinear iterative procedure has been proposed and its optimality has been established, in [24], multilevel iterative methods have been studied for Richards' equation, in [10], two-level domain decomposition methods have been proposed and analyzed. To the best of our knowledge, the techniques developed in the previous works have not considered the case of highly heterogeneous conductivity fields, which is the main objective of this paper. The proposed iterative procedure involves outer iterations and inner iterations, a technique that is commonly used in the literature. Outer iterations are designed to handle nonlinearities by linearizing the equation around the previous state. The simplest is Picard iteration that is described by $\operatorname{div}(k(x)\lambda(x,u^n)\nabla u^{n+1}) = f$, where n denotes the outer iteration number. For every outer iteration n, a linear problem needs to be solved. For the solution of the linear problem, we employ two-level domain decomposition preconditioners within conjugate gradient (CG) iterative technique. Both inner and outer iteration can, in general, depend on the contrast and small scales. One of our main goals is to construct an iterative process that converges independently of both, the small scales and the contrast. In particular, we show that the robust iterative techniques designed for a linear system can be re-used for every outer iteration if λ is a smooth function. Therefore, it is important to use efficient preconditioners for solving linear systems arising in approximation of problems with highly heterogeneous coefficients. Such preconditioners, designed in the earlier works [15, 17, 18], are discussed below and described in Section 3.

For every outer iteration, the resulting linear system on the fine scale is solved using a two-level domain decomposition preconditioner (e.g., [32, 25]), which involves local (subdomain) and global (coarse) problems. The number of iterations required by domain decomposition preconditioners is typically affected by the contrast in the media properties (e.g., [25, 32]) that are within each coarse grid block. Because of the complex geometry of fine-scale features, it is often impossible to separate low and high conductivity regions into different coarse grid blocks. Consequently, without proper preconditioner, the number of iterations can be very large, which substantially reduces the efficiency of the iterative method, particularly for nonlinear flows.

In this paper, for every outer iteration we use the preconditioners designed in [15, 17]. The main idea of these preconditioners consists of augmenting the coarse space in the domain decomposition methods. In particular, a coarse space based on local spectral problems using multiscale functions is constructed. We prove that when the coarse space in the domain decomposition methods includes these eigenfunctions, the condition number of the preconditioned matrix is bounded independently of the contrast. The choice of multiscale spaces is important

to achieve small dimensional coarse spaces. By incorporating small-scale localizable features of the solution into initial multiscale basis functions, we have shown that one can achieve small dimensional coarse spaces without sacrificing the convergence properties of the preconditioners. Initial multiscale spaces can employ constructions proposed for multiscale finite element methods in [12, 14, 22, 23].

We show that both, the number of outer iterations and the number of inner iterations, are bounded independently of physical parameters, such as the contrast and small spatial scales. We first prove that under some assumptions the number of outer iterations depends on the contraction constant that is independent of the contrast in the conductivity field. Our reasoning takes into account the high variations of the contrast in the conductivity field and follows the standard for such nonlinear problems technique, e.g., [4]. As for inner iterations, we use two-level preconditioners developed in [15, 17] that provide, independent of the contrast, condition number for every outer iteration. We use the same preconditioner for every outer iteration repeatedly without sacrificing the convergence of the overall method.

We note that one can use Kirchhoff's potential (see, e.g. [7, p. 29-31]) to transform the original equation into a linear equation for the potential. However, this technique becomes cumbersome when $\lambda(x,u)$ depends on x and does not have an explicit form (e.g., given via a graph interpolation). Moreover, the difficulty of inversion of Kirchhoff's potential still needs to be performed and the extensions to time-dependent problems can become complicated.

We test our methodology on a number of numerical examples for various nonlinear models. We consider two different heterogeneous permeability fields and vary the contrast over four orders in magnitude. Our numerical results show that the number of outer iterations does not depend on the contrast. Moreover, the number of inner iterations on every outer iteration does not depend on the contrast if an appropriate preconditioner is chosen. We also test two-level domain decomposition preconditioner when the coarse space includes only the initial multiscale basis functions. In this case, the number of iterations at every outer iteration grows as the contrast increases.

The paper is organized as follows. In Section 2, we introduce the problem. Section 3 is devoted to the description of robust preconditioners. Some of the proofs are presented in the Appendix. In Section 4 we present numerical results and, finally, in Section 5 we draw some conclusions.

2. Problem setting

2.1. **Weak Formulation.** We multiply equation (3) by a test function $v \in H_0^1(\Omega)$ and integrate over the domain Ω. After applying the divergence theorem, we get that the solution u satisfies the following integral identity

$$\int_\Omega k(x)\lambda(x,u)\nabla u \nabla v dx \;\; = \;\; \int_\Omega f v dx, \quad \text{for all } v \in H_0^1(\Omega).$$

Now we define the space $V = H_0^1(\Omega)$, set of all functions with square integrable generalized derivatives of first order vanishing on the boundary $\partial\Omega$, the form $a(\cdot,\cdot;\cdot)$

$$a(u,v;w) = \int_\Omega k(x)\lambda(x,w)\nabla u \nabla v dx, \tag{4}$$

and the functional $F(\cdot)$

$$F(v) = \int_\Omega f v dx. \tag{5}$$

Then the variational form of (3) is to find $u \in V$ such that

$$a(u, v; u) = F(v), \qquad \text{for all } v \in V. \tag{6}$$

2.2. **Finite Element Discretization.** Let $\mathcal{T}_h$ be a triangulation of the domain Ω into a finite number of triangular (tetrahedral) elements. We assume that $\mathcal{T}_h$ is quasiuniform and regular; see [9]. Let V^h be the finite dimensional subspace of V of piece-wise polynomials with respect to $\mathcal{T}_h$. Let $u_h \in V^h$ be a solution of the following discrete problem.

$$a(u_h, v; u_h) = F(v), \qquad \text{for all } v \in V^h. \tag{7}$$

We know that under suitable conditions, one can ensure the existence of a solution to the above equation. Define the nonlinear map $T_h : V^h \to V^h$ by

$$a(T_h u_h, v; u_h) = F(v), \qquad \text{for all } v \in V^h. \tag{8}$$

This is well defined, since $u_h \in V^h$.

2.3. **A nonlinear fixed point iteration.** In this section we describe a robust numerical method to approximate the numerical solutions of the Richards' equation (7). We use a fixed point iteration based on the contractivity of the mapping T_h defined in (8). The numerical solution u_h can be approximated to an arbitrary accuracy using Picard iteration.

Starting with an initial guess $u_h^0 \in V^h$, we define the nonlinear fixed point iteration by

$$u_h^{n+1} = T_h u_h^n.$$

That is, given u_h^n, the next approximation u_h^{n+1} is the solution of the linear elliptic equation

$$a(u_h^{n+1}, w; u_h^n) = F(w), \quad \text{for all } w \in V^h. \tag{9}$$

In order to define the solution method, we reformulate the problem (9) in terms of the linear operator $A^n : V^h \to V^h$ defined for any given $u_h^n \in V^h$ as

$$a(v, w; u_h^n) = (A^n v, w), \quad \text{for all } v, w \in V^h, \tag{10}$$

where $(\cdot, \cdot)$ is the standard L^2-inner product in V^h. In a similar manner, we present the linear functional $F(w)$ in the form

$$F(w) = (b, w), \quad \text{for all } w \in V^h. \tag{11}$$

Obviously, b is the L^2-projection of the right hand side f of (3) on V^h. Then the equation (9) can be rewritten in the following operator form

$$A^n u_h^{n+1} = b. \tag{12}$$

Note that equation (9) (and its operator counterpart (12)) is an approximation of the linear equation $-\text{div}(k(x)\lambda(x, u_h^n)\nabla u_h^{n+1}) = f$ with u_h^n being the previous iterate. It is known that the presence of the high-contrast coefficient $k(x)$ makes it computationally difficult to construct appropriated robust linear solvers for computing u_h^{n+1}. Moreover, taking into account the contractivity of the operator T_h, in order to get a robust method to compute the solution of the Richards' equation (8), we only need a robust method for solving the linear problem (9). Because of the small scales and high contrast in the conductivity field, the solution of this system (of size proportional the fine grid points) is prohibitively expensive. Therefore, an adequate robust iterative method is needed.

The construction of robust solvers for high-contrast linear elliptic equation has been considered by many authors. We will use as a preconditioner a two-level domain decomposition method proposed in [15, 17, 18], which involves solutions of appropriate local spectral problems.

If B^{-1} is the preconditioner, our goal is to have the condition number of $B^{-1}A^n$ bounded independent of the contrast and n (i.e, independent of u_h^n). Now we describe a construction of such preconditioner for (12), which will give a robust, with respect to the contrast, method for Richards' equation.

3. Finite element discretization and two level domain decomposition preconditioner

3.1. **Finite element approximation and local spaces.** First, we provide an overview of the use of domain decomposition techniques for constructing preconditioners for multiscale finite element approximations of high-contrast elliptic equations (cf., [15, 17, 18, 19, 20]). For an extension to multilevel methods, we refer to [16]. Next, we briefly describe a two-level domain decomposition setting that we use and introduce the local spaces and the coarse space.

Let $\mathcal{T}_H$ and $\mathcal{T}_h$ be coarse and fine partitions of Ω into finite elements K (or nonoverlapping subdomains) that consists of triangles, quadrilaterals, etc.. We assume that the coarse elements of $\mathcal{T}_H$ consist of a number of fine elements from $\mathcal{T}_h$. Practically, we first introduce the coarse-grid $\mathcal{T}_H$ and then obtain the fine grid $\mathcal{T}_h$ by partitioning each coarse element into a number of smaller ones. Let χ_i be the nodal basis of the standard finite element space with respect to the coarse triangulation $\mathcal{T}_H$. We denote by N_v the number of coarse nodes, by $\{y_i\}_{i=1}^{N_v}$ the vertices of the coarse mesh $\mathcal{T}_H$, and define a neighborhood of each node y_i by

$$\omega_i = \bigcup \{K_j \in \mathcal{T}_H;\ y_i \in \overline{K}_j\}. \tag{13}$$

Let $V_0^h(\omega_i) \subset V^h$ be the set of finite element functions with support in ω_i and $R_i^T : V_0^h(\omega_i) \to V^h$ denote the extension by zero operator.

We define, for later use, the one level additive preconditioner (e.g. [25, 32])

$$B_1^{-1} = \sum_{i=1}^{N_v} R_i^T (A_i^0)^{-1} R_i, \tag{14}$$

where the operators $A_i^0 : V_0^h(\omega_i) \to V_0^h(\omega_i)$ are defined by

$$(A_i^0 v, w) = a(v, w; u_h^0), \quad \text{for all } v, w \in V_0^h(\omega_i),\ i = 1, \ldots, N_v. \tag{15}$$

The application of the preconditioner B_1^{-1} involves $(A_i^0)^{-1}$ which means solving local problems subdomain-wise in each iteration. The operator A_i^0, defined by the bilinear form $a(\cdot, \cdot; u_h^0)$ restricted to $V_0^h(\Omega_i')$, is local and invertible.

3.2. **Coarse space construction.** For given M_c number of linearly independent functions $\{\Phi_i\}_{i=1}^{M_c}$ associated with the coarse mesh $\mathcal{T}_H$ (these will be introduced later), we define a coarse space V_0 by

$$V_0 = \text{span}\{\Phi_i\}_{i=1}^{M_c}. \tag{16}$$

Below we shall give three choices of sets $\{\Phi_i\}_{i=1}^{M_c}$, that have been already used in the construction of a robust preconditioner for A^n. These are: (1) multiscale coarse space (see, e.g. [12] and the references therein), (2) energy minimizing coarse space (see, e.g. [35]), and (3) a coarse space with local spectral information, (see, e.g. [15, 17, 18]). On an abstract level, the main assumption is that $\Phi_i \in V^h$, but the support of each Φ_i is related to the coarse mesh $\mathcal{T}_H$ so that $M_c << \dim V^h$. Below we refer to the Φ_i's as coarse-scale basis functions. The coarse space V_0 defines an operator

$$A_c : V_0 \to V_0, \quad (A_c v, w; u_h^0) = a(v, w; u_h^0),\ \forall v, w \in V_0.$$

Note that if $R_c^T : V_0 \to V^h$ is the natural interpolation operator, then we have

$$A_c = R_c A^0 R_c^T \quad \text{with } A^0 \text{ defined by (10) for } n = 0. \tag{17}$$

Note that the operator A_c uses the initial guess $u_h^0 \in V^h$ and is constructed only once at the beginning of the fixed point nonlinear iteration. Likewise, the coarse basis functions $\{\Phi_j\}_{j=1}^{M_c}$ are related to the form $a(\cdot,\cdot;u_h^0)$ and are constructed only one time. These can be regarded as a preprocessing step. Once the coarse space V_0 is constructed and the coarse-scale operator A_c is defined, we can use the two level additive preconditioner of the form

$$B^{-1} = R_c^T A_c^{-1} R_c + \sum_{i=1}^{N_v} R_i^T (A_i^0)^{-1} R_i = R_c^T A_c^{-1} R_c + B_1^{-1}. \tag{18}$$

The preconditioner B^{-1} involves solving one coarse-scale system and N_v local problems in each overlapping subdomain ω_i, $i = 1, \ldots, N_v$. The goal is to reduce the number of iterations in the iterative procedure, e.g., a preconditioned conjugate gradient. An appropriate construction of the coarse space V_0 plays a key role in obtaining robust iterative domain decomposition method. In the next Section 3.3 we present examples of such coarse space constructions. We summarize the fixed point iteration in Algorithm 1.

Algorithm 1 Fixed point iteration

1: Initialize: Choose $u_h^0 \in V^h$ and compute the residual $r^0 = b - A^0 u_h^0$.
2: Construct the coarse basis $\{\Phi_j\}$, the coarse space V_0 in (16), and the coarse operator A_c in (17) .
3: **for** $n = 1, 2, \ldots$ until convergence **do**
4: Set the linear system $A^n u_h^{n+1} = b$ (see (12)).
5: Using PCG with preconditioner B^{-1} in (18) solve the linear system in 4: to get u_h^{n+1}.
6: Compute the residual $r^{n+1} = b - A^{n+1} u_h^{n+1}$.
7: **end for**

Remark 1. *In the general domain decomposition method setting the overlapping subdomains $\{\omega_i\}$ could be chosen independently of the coarse triangulation $\mathcal{T}^H$. However, for the purpose of this paper, we will only consider the partition introduced above.*

3.3. **Some multiscale coarse spaces.** In this subsection we review several possibilities for construction of coarse basis functions that have been used to design two-level preconditioners that are robust with respect to the contrast.

3.3.1. *Linear boundary conditions multiscale coarse spaces.* Let χ_i^H be the nodal basis of the standard finite element space with respect to the coarse triangulation $\mathcal{T}_H$. We define multiscale finite element basis function χ_i^{ms} that coincides with χ_i^H on the boundaries of the coarse partition. Namely, for each $K \subset \omega_i$

$$\int_K k \nabla \chi_i^{ms} \nabla v dx = 0, \quad \forall v \in V^h \cap V_0^h(\omega_i) \text{ and } \chi_i^{ms} = \chi_i^H \text{ on } \partial K. \tag{19}$$

This means that χ_i^H is an approximation in the fine-grid space of the boundary value problem

$$-\text{div}(k \nabla \chi_i^{ms}) = 0 \text{ in } K \subset \omega_i, \quad \chi_i^{ms} = \chi_i^H \text{ in } \partial K, \quad \text{for all } K \subset \omega_i, \tag{20}$$

where K is a coarse grid element within ω_i. Then we define

$$V_0^{ms} = \text{span}\{\chi_i^{ms}\}. \tag{21}$$

Note that multiscale basis functions coincide with standard finite element basis functions on the boundaries of coarse grid blocks, while are oscillatory in the interior of each coarse grid block. Even though the choice of χ_i^H can be quite arbitrary, our main assumption is that the basis functions satisfy the leading order homogeneous equations when the right hand side f is a smooth function (e.g., L_2 integrable). We remark that the MsFEM formulation allows one to take advantage of scale separation. In particular, K can be chosen to be a volume smaller than the coarse grid. Various other boundary conditions have been introduced and analyzed in the literature, see [12] and references therein. For example, in [23], reduced boundary conditions are found to be efficient in many porous media applications.

3.3.2. *Energy minimizing coarse spaces.* Coarse basis functions can be obtained by minimizing the energy of the basis functions subject to a global constraint (see, [35]). More precisely, one can use the partition of unity functions $\{\chi_i^{em}\}_{i=1}^{N_v}$, with N_v being the number of coarse nodes, that provide the least energy. This can be accomplished by solving

$$\min \sum_{i=1}^{N_v} \int_{\omega_i} k|\nabla \chi_i^{em}|^2, \tag{22}$$

subject to the constraint $\sum_i \chi_i^{em} = 1$ with $\text{supp}(\chi_i^{em}) \subset \omega_i$, $i = 1, \ldots, N_v$. Note that $\sum_i \chi_i^{em} = 1$ is a global constraint though it is not tied to any particular global fields unlike the methods discussed previously. One can solve (22) following a procedure discussed in [35] and then define the coarse space

$$V_0^{em} = \text{span}\{\chi_i^{em}\}. \tag{23}$$

We note that the computation of these basis functions requires the solution of a global linear system, a procedure more expensive compared to the local computation of multiscale finite element basis functions with linear boundary conditions χ_i^{ms}.

3.3.3. *A coarse space with local spectral information.* We motivate the choice of the coarse spaces based on the analysis presented in [15, 17, 18]. First, we briefly review the results of [15, 17, 18]. For fixed ω_i consider the eigenvalue problem

$$-\text{div}(k\nabla \psi_\ell^{\omega_i}) = \mu_\ell^{\omega_i} \widetilde{k} \psi_\ell^{\omega_i}, \tag{24}$$

where $\mu_\ell^{\omega_i}$ and $\psi_\ell^{\omega_i}$ are eigenvalues and eigenvectors in ω_i and $\widetilde{k}$ is defined by

$$\widetilde{k} = \frac{1}{H^2} k \sum_{j=1}^{N_v} |\nabla \chi_j^{in}|^2. \tag{25}$$

We recall that χ_j^{in} (simply denoted by χ_j in further discussions) are the initial multiscale basis functions (either multiscale basis functions with linear boundary conditions or energy minimizing basis functions) and N_v is the number of the coarse nodes. The eigenvalue problem considered above is solved with zero Neumann boundary condition and understood in a discrete setting. Assume eigenvalues are given by

$$\mu_1^{\omega_i} \leq \mu_2^{\omega_i} \leq \ldots.$$

Basis functions are computed by selecting a number of eigenvalues (starting with small ones) and multiplying corresponding eigenvectors by χ_i. Thus, multiscale space is defined for each i as the span of $\chi_i \psi_\ell^{\omega_i}$, $\ell = 1, ..., L_i$, where L_i is the number of selected eigenvectors (see Figure 1 for an illustration).

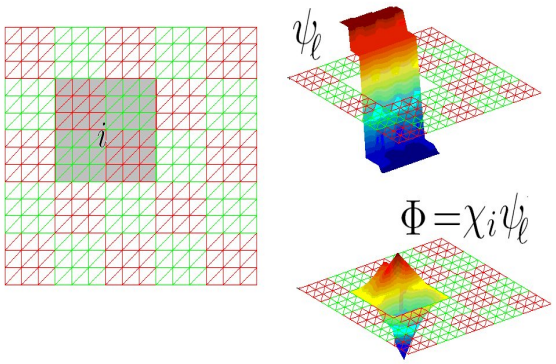

FIGURE 1. Illustration of basis construction

We note that $\{\omega_i\}_{y_i \in \mathcal{T}^H}$ is a covering of Ω. Let $\{\chi_i\}_{i=1}^{N_v}$ be a partition of unity subordinated to the covering $\{\omega_i\}$ such that $\chi_i \in V_0^h(\omega_i)$ and $|\nabla \chi_i| \leq \frac{1}{H}$, $i = 1, \ldots, N_v$. Define the set of coarse basis functions

$$\Phi_{i,\ell} = I^h(\chi_i \psi_\ell^{\omega_i}), \qquad \text{for } 1 \leq \ell \leq L_i \text{ and } 1 \leq i \leq N_v, \tag{26}$$

where I^h is the fine-scale nodal value interpolation and L_i is an integer number specified for each $i = 1, \ldots, N_v$. Note that in this case, there might be several basis functions per coarse node. The number of basis functions per node is defined via the eigenvalue problem (24). Denote by V_0 the *local spectral multiscale* space

$$V_0^{lsm} = \text{span}\{\Phi_{i,\ell} : 1 \leq \ell \leq L_i \text{ and } 1 \leq i \leq N_v\}. \tag{27}$$

3.4. **Condition number estimates.** In this section, we present a theoretical result which shows that the number of outer iterations is independent of the contrast. First, for a given $\mathcal{K} > 0$ we introduce the ball

$$V_h^{\mathcal{K},p} := \{v \in V_h : \|v\|_{W_p^1} \leq \mathcal{K}\}. \tag{28}$$

The following three assumptions are used in the proofs of Theorems 1, 2, and 3.

Assumption 1.

(A) $C_0 \leq k(x) \leq M$, *where* C_0, *and* M *is a constant.*

(B) The function $\lambda(x, u)$ *satisfies the following conditions.*

- *(a)* $\lambda(x, u)$ *is Lipschitz continuous with respect to* u, *i.e., there exists a constant* C_1 *such that* $|\lambda(x, u) - \lambda(x, v)| \leq C_1|u - v|$, *for all* $u, v \in V$, $x \in \Omega$,
- *(b)* $\lambda(x, u)$ *is bounded above, i.e. there is a constant* C *such that* $\lambda(x, u) \leq C$ *for all* $x \in \Omega$ *and* $u \in L^\infty(\Omega)$
- *(c)* $\lambda(x, u)$ *is bounded below, i.e. there is a constant* C_2 *such that* $0 < C_2 \leq \lambda(x, u)$ *for all* $x \in \Omega$ *and* $u \in V$.

(C) See (43).

Under these assumptions, we show the following theorems concerning the existence of the solution and the boundedness of the contraction constant.

Theorem 1. *Under the Assumption 1 (A) and (B), there are constants* $\alpha < \infty, h_0 > 0$ *and* $\epsilon > 0$ *such that for all* $0 < h \leq h_0$ *and* $u_h \in V^h$

$$|u_h|_{W_p^1(\Omega)} \leq \alpha \sup_{0 \neq v_h \in V^h} \frac{a(u_h, v_h; \cdot)}{|v_h|_{W_q^1(\Omega)}}, \quad \textit{with} \quad a(u, v; \cdot) = \int_\Omega k \nabla u \nabla v \, dx, \tag{29}$$

whenever $|2-p| \leq \epsilon$, q *is the dual index to* p, $\frac{1}{p}+\frac{1}{q}=1$ *and* $|\cdot|_{W_q^1(\Omega)}$ *is a semi-norm in* $W_q^1(\Omega)$.

Theorem 2. *Let the Assumption 1 (A), (B), and (C) hold. Then (a) there exists* $\mathcal{K}>0, p>2, h_0>0$, *and* $\delta>0$ *such that for all* F *with* $\|F\|_{W_p^{-1}} \leq \delta$, T_h *maps* $V_h^{\mathcal{K},p}$ *into itself for all* $0<h\leq h_0$ *and by Browder fixed point Theorem, there exists a solution* $\tilde{u}_h$ *of equation (7) and it satisfies*

$$T_h\tilde{u}_h = \tilde{u}_h. \tag{30}$$

(b) The map $T_h : V_h^{\mathcal{K},p} \to V_h^{\mathcal{K},p}$ *is a contraction and the contraction constant is independent of the contrast.*

Theorem 3. *Under the assumptions of Theorem 1, we have* $cond(B^{-1}A^n) \leq C$, *where* C *is independent of the contrast.*

The proofs of these theorems are presented in Appendix A.

4. Numerical results

In this section we present some representative numerical examples. We solve the Richards' equation (7) in $\Omega=[0,1]\times[0,1]$ with $f(x)=1$ and homogeneous Dirichlet boundary conditions. We consider several models for the hydraulic conductivity: the Haverkamp, van Genuchten, and Exponential model, (see, e.g. [7, 21, 33, 27]), as introduced below. The coarse mesh $\mathcal{T}_H$ is obtained by dividing Ω into a 10×10 mesh. The fine triangulation is obtained by dividing each coarse-mesh element into 10×10 squares and further dividing each square into two triangles. Thus, the fine-mesh step size is $h=1/100$. In all the numerical experiments we use the initial approximation for the iterative process u_h^0 that solves

$$a(u_h^0, v; 0) = F(v), \qquad \text{for all } v \in V^h. \tag{31}$$

We apply the Algorithm (1). As stated in Algorithm (1) we use the preconditioner B^{-1} in (18) with three different coarse spaces:

(1) V_0^{ms} described in Section 3.3.1. In this case B^{-1} is denoted by B_{ms}^{-1};
(2) V_0^{em} described in Section 3.3.2. In this case B^{-1} is denoted by B_{em}^{-1};
(3) V_0^{lsm} described in Section 3.3.3. In this case B^{-1} is denoted by B_{lsm}^{-1}.

We study the performance of Algorithm 1 with initial guess u_h^0 and preconditioners B_{ms}^{-1}, B_{em}^{-1}, and B_{lsm}^{-1}. We consider different permeabilities with complex high-contrast configurations, see Figure 2. A number of parameter values in the nonlinearity of the hydraulic conductivity are tested in our simulations. In particular, for each experiment we chose a different set of parameters for the model and a set of contrast values for the hydraulic conductivity. We note that, for each outer iteration in Algorithm 1 we have a PCG iteration. The inner PCG iteration is convergent when the initial residual is reduced by a factor of $tol_{in} = 1e-10$ while the outer tolerance is set to $tol_{out} = 1e-8$.

We consider the following indicators for the performance of the preconditioners:

- Coarse space dimension;
- The number of outer iterations of the nonlinear fixed point iteration (R-iter);
- The maximum and minimum number of inner PCG iterations over all outer iterations (CG-iter) and the estimated maximum condition numbers (Cond).

We also verify numerically our main assumption in the proof of Theorem 1. That is, for every outer iteration update we compute $\|\sqrt{k}|\nabla u|\|_p^p = \int_D (\sqrt{k}|\nabla u|)^p\, dx$, $p=1,2,3,\ldots,10$. We observe that this quantity remains bounded in all experiments.

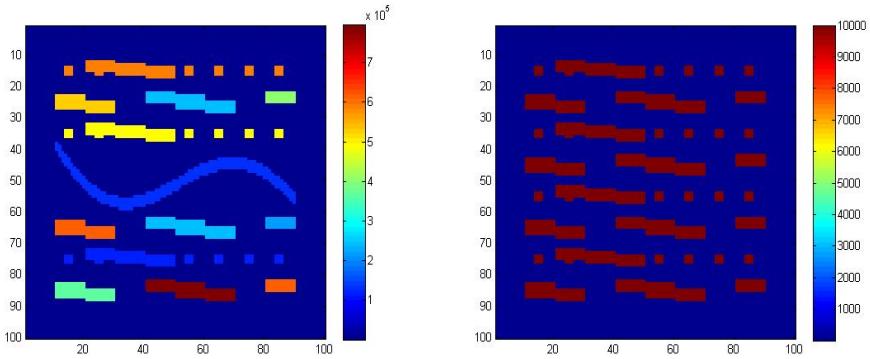

FIGURE 2. (Left): Conductivity field 1. Blue designates the regions where the coefficient is 1 and other colors designates the regions where the coefficient is a random number between η and $10 * \eta$. (Right): Conductivity field 2. Blue designates the regions where the coefficient is 1 and red designates the regions where the coefficient is η.

4.1. **Haverkamp model.** First, we will study the Haverkamp model. In this model, (see, e.g. [21]), the hydraulic conductivity is given by

$$k(x,u) = k_s(x)\frac{A}{A + (|u|/B)^{\gamma}}. \tag{32}$$

We present the first set of numerical results in Tables 1 and 2. We use the preconditioner B_{ms}^{-1} based on the coarse space V_0^{ms}. We observe from these tables that the numbers of outer iterations do not change when the contrast value η increases. However, the condition number of the preconditioned system grows as η increases. We also observe that the quantity $\|\sqrt{k}|\nabla u|\|_p^p, p = 1, 2, 3, \ldots, 10$, that is related to the number of outer iterations, is bounded. We observe that the number of outer iterations is larger when B and γ (see (32)) decrease. This is because the smaller values of B and γ increase the magnitude of the conductivity that comes from its nonlinear component. Comparing Tables 1 and 2 that use different conductivity fields, we see that the condition numbers in Table 2 are smaller than the condition numbers in Table 1. This is because conductivity field 2 (see Figure 2) has simpler heterogeneity structure compared to conductivity field 1.

Next, we repeat the above numerical experiments using the preconditioner B_{em}^{-1} based on the coarse space V_0^{em}. Numerical results are presented in Tables 3 and 4. We observe that, as before, the number of outer iterations is fixed with increasing η. On the other hand, the condition number of the PCG iteration grows as the contrast increases. This condition number is much larger compared to the case when spectral basis functions are used as presented in the next tables.

Further, we show the numerical experiment using the preconditioner B_{lsm}^{-1} based on the spectral coarse space V_0^{lsm}. Numerical results are presented in Tables 5 and 6. As before, we observe that the number of outer iterations is independent of the contrast. We observe that the condition number is also independent of the contrast. Note that the condition number is substantially smaller than the one of the preconditioned system using B_{ms}^{-1} or B_{em}^{-1}. In general, the number of inner PCG iterations is much smaller compared to those when other coarse spaces are used.

4.2. **van Genuchten Model.** Next, we consider *the Van Genuchten model* (see [33]) that is one of widely used empirical constitutive relations. In this model, the hydraulic conductivity is

	$A=1,\ B=1,\ \gamma=1$				$A=1,\ B=0.01,\ \gamma=0.5$			
η	R-iter	CG-iter	Max Cond	$\|(\sqrt{k}\|\nabla u\|)\|_p^p$	R-iter	CG-iter	Max Cond	$\|(\sqrt{k}\|\nabla u\|)\|_p^p$
10^3	4	$119, 124$	$1.1e+3$	0.12	11	$131, 139$	$1.4e+3$	0.12
10^4	4	$166, 178$	$1.1e+4$	0.12	11	$179, 199$	$1.4e+4$	0.12
10^5	4	$224, 224$	$1.1e+5$	0.12	11	$224, 224$	$1.4e+5$	0.12
10^6	4	$278, 278$	$1.1e+6$	0.12	11	$278, 278$	$1.4e+6$	0.12

TABLE 1. Numerical results for preconditioner B_{ms}^{-1}. Here we use the Haverkamp model $k(x,u) = k(x)\frac{A}{A+(|u|/B)^\gamma}$ with k depicted in the left picture of Figure 2. The coarse space dimension is 81.

	$A=1,\ B=1,\ \gamma=1$				$A=1,\ B=0.01,\ \gamma=0.5$			
η	R-iter	CG-iter	Max Cond	$\|(\sqrt{k}\|\nabla u\|)\|_p^p$	R-iter	CG-iter	Max Cond	$\|(\sqrt{k}\|\nabla u\|)\|_p^p$
10^3	4	$113, 113$	$2.6e+2$	0.13	11	$107, 123$	$3.9e+2$	0.13
10^4	4	$163, 171$	$2.5e+3$	0.13	11	$180, 193$	$3.6e+3$	0.13
10^5	4	$224, 232$	$2.5e+4$	0.13	11	$238, 255$	$3.6e+4$	0.13
10^6	4	$288, 295$	$2.5e+5$	0.13	11	$308, 324$	$3.6e+5$	0.13

TABLE 2. Numerical results for preconditioner B_{ms}^{-1}. Here we use the Haverkamp model $k(x,u) = k(x)\frac{A}{A+(|u|/B)^\gamma}$ with k depicted in the right picture of Figure 2. The coarse space dimension is 81.

	$A=1,\ B=1,\ \gamma=1$				$A=1,\ B=0.01,\ \gamma=0.5$			
η	R-iter	CG-iter	Max Cond	$\|(\sqrt{k}\|\nabla u\|)\|_p^p$	R-iter	CG-iter	Max Cond	$\|(\sqrt{k}\|\nabla u\|)\|_p^p$
10^3	3	$83, 83$	$1.3e+2$	0.12	8	$90, 102$	$1.9e+2$	0.12
10^4	3	$88, 88$	$2.5e+2$	0.12	8	$95, 109$	$3.9e+2$	0.12
10^5	3	$89, 90$	$3.0e+2$	0.12	8	$97, 113$	$4.6e+2$	0.12
10^6	3	$95, 103$	$3.1e+2$	0.12	8	$103, 115$	$4.7e+2$	0.12

TABLE 3. Numerical results for preconditioner B_{em}^{-1}. Here we use the Haverkamp model $k(x,u) = k(x)\frac{A}{A+(|u|/B)^\gamma}$ with k depicted in the left picture of Figure 2. The coarse space dimension is 81.

	$A=1,\ B=1,\ \gamma=1$				$A=1,\ B=0.01,\ \gamma=0.5$			
η	R-iter	CG-iter	Max Cond	$\|(\sqrt{k}\|\nabla u\|)\|_p^p$	R-iter	CG-iter	Max Cond	$\|(\sqrt{k}\|\nabla u\|)\|_p^p$
10^3	3	$90, 90$	$1.6e+2$	0.13	8	$84, 98$	$2.7e+2$	0.13
10^4	3	$94, 94$	$3.7e+2$	0.13	8	$88, 102$	$6.2e+2$	0.13
10^5	3	$95, 95$	$4.2e+2$	0.13	8	$89, 103$	$7.1e+2$	0.13
10^6	3	$96, 96$	$4.3e+2$	0.13	8	$91, 104$	$7.2e+2$	0.13

TABLE 4. Numerical results for preconditioner B_{em}^{-1}. Here we use the Haverkamp model $k(x,u) = k(x)\frac{A}{A+(|u|/B)^\gamma}$ with k depicted in the right picture of Figure 2. The coarse space dimension is 81.

given by

$$k(x,u) = k_s(x)\frac{\{1-(\alpha|u|/B)^{n-1}[1+(\alpha|u|)^n]^{-m}\}^2}{[1+(\alpha|u|)^n]^{\frac{m}{2}}}. \tag{33}$$

	$A=1,\ B=1,\ \gamma=1$				$A=1,\ B=0.01,\ \gamma=0.5$			
η	R-iter	CG-iter	Max Cond	$\|(\sqrt{k}\|\nabla u\|)\|_p^p$	R-iter	CG-iter	Max Cond	$\|(\sqrt{k}\|\nabla u\|)\|_p^p$
10^3	4	$34, 34$	6.9	0.13	8	$37, 39$	9.6	0.13
10^4	4	$35, 35$	7.0	0.13	8	$39, 41$	9.7	0.13
10^5	4	$35, 37$	7.0	0.13	8	$40, 42$	9.7	0.13
10^6	4	$36, 36$	7.0	0.13	8	$41, 44$	9.7	0.13

TABLE 5. Numerical results for preconditioner B_{lsm}^{-1}. Here we use the Haverkamp model $k(x,u) = k(x)\frac{A}{A+(|u|/B)^\gamma}$ with k depicted in the left picture of Figure 2. The coarse space dimension is 166.

	$A=1,\ B=1,\ \gamma=1$				$A=1,\ B=0.01,\ \gamma=0.5$			
η	R-iter	CG-iter	Max Cond	$\|(\sqrt{k}\|\nabla u\|)\|_p^p$	R-iter	CG-iter	Max Cond	$\|(\sqrt{k}\|\nabla u\|)\|_p^p$
10^3	3	$31, 31$	6.2	0.13	8	$35, 37$	8.1	0.13
10^4	3	$33, 33$	6.3	0.13	8	$36, 37$	8.0	0.13
10^5	3	$33, 33$	6.3	0.13	8	$38, 43$	8.0	0.13
10^6	3	$34, 34$	6.3	0.13	8	$38, 41$	8.0	0.13

TABLE 6. Numerical results for preconditioner B_{lsm}^{-1}. Here we use the Haverkamp model $k(x,u) = k(x)\frac{A}{A+(|u|/B)^\gamma}$ with k depicted in the right picture of Figure 2. The coarse space dimension is 184.

As before, we will present numerical results for all three coarse spaces. First, in Tables 7 and 8 we present the numerical results for the preconditioner B_{ms}^{-1}. We observe that the number of outer iterations is smaller compared to the other two models. The number of outer iterations stays the same while increasing η. On the other hand, the condition number of the linearized system increases as η increases. We observe that the value $\|\sqrt{k}|\nabla u|\|_p^p, p = 1, 2, 3, \ldots, 10$ is bounded independent of the contrast. Now we compare Table 7 and Table 8 for two different conductivity fields depicted in Figure 2. We observe that the condition numbers presented in Table 8 is smaller than those presented in Table 7 which is consistent with our previous observations.

Numerical results for the preconditioner B_{em}^{-1} are presented in Tables 9 and 10, while numerical results for the preconditioner B_{lsm}^{-1} are presented in Tables 11 and 12. As before, we observe that the number of outer iteration does not change with η increasing. However, the condition number of the inner iteration is increasing for B_{em}^{-1}, while the condition number of the inner iteration does not change (and is much smaller) for B_{lsm}^{-1}.

4.3. **Exponential Model.** Finally, we present numerical results for the exponential model. Here the hydraulic conductivity depend exponentially on the pressure head u, that is,

$$k(x,u) = k_s(x)e^{\alpha u/B}. \tag{34}$$

This nonlinear equation can also be derived by homogenizing Stokes equation in porous media when the fluid viscosity exponentially depends on the pressure [27].

We present the first set of numerical results in Tables 13 and 14. First, we use the preconditioner B_{ms}^{-1} based on the coarse space V_0^{ms}. We observe that the number of the outer iterations does not change when the contrast η increases. However, the condition number of the preconditioned system increases proportional to η. We also observe that the quantity

	$\alpha = 0.005$, $B = 1$, $n = 2$, $m = 0.5$				$\alpha = 0.01$, $B = 1$, $n = 4$, $m = 0.75$			
η	R-iter	CG-iter	Max Cond	$\|(\sqrt{k}\|\nabla u\|)\|_p^p$	R-iter	CG-iter	Max Cond	$\|(\sqrt{k}\|\nabla u\|)\|_p^p$
10^3	2	$116, 116$	$1.1e+3$	0.13	2	$115, 116$	$1.1e+3$	0.13
10^4	2	$168, 168$	$1.1e+4$	0.13	2	$174, 174$	$1.1e+4$	0.13
10^5	2	$219, 219$	$1.1e+5$	0.13	2	$219, 219$	$1.1e+5$	0.13
10^6	2	$273, 290$	$1.1e+6$	0.13	2	$267, 272$	$1.1e+6$	0.13

TABLE 7. Numerical results for preconditioner B_{ms}^{-1}. Here we use the van Genuchten model $k(x,u) = k(x)\frac{\{1-(\alpha(|u|/B))^{n-1}[1+(\alpha(|u|/B))^n]^{-m}\}^2}{[1+(\alpha(|u|/B))^n]^{m/2}}$ with k depicted in the left picture of Figure 2. The coarse space dimension is 81.

	$\alpha = 0.005$, $B = 1$, $n = 2$, $m = 0.5$				$\alpha = 0.01$, $B = 1$, $n = 4$, $m = 0.75$			
η	R-iter	CG-iter	Max Cond	$\|(\sqrt{k}\|\nabla u\|)\|_p^p$	R-iter	CG-iter	Max Cond	$\|(\sqrt{k}\|\nabla u\|)\|_p^p$
10^3	2	$98, 99$	$2.5e+2$	0.13	2	$99, 99$	$2.5e+2$	0.13
10^4	2	$134, 134$	$2.5e+3$	0.13	2	$160, 160$	$2.5e+3$	0.13
10^5	2	$183, 184$	$2.5e+4$	0.13	2	$219, 223$	$2.5e+4$	0.13
10^6	2	$222, 225$	$2.5e+5$	0.13	2	$286, 287$	$2.5e+5$	0.13

TABLE 8. Numerical results for preconditioner B_{ms}^{-1}. Here we use the van Genuchten model $k(x,u) = k(x)\frac{\{1-(\alpha(|u|/B))^{n-1}[1+(\alpha(|u|/B))^n]^{-m}\}^2}{[1+(\alpha(|u|/B))^n]^{m/2}}$ with k depicted in the right picture of Figure 2. The coarse space dimension is 81.

	$\alpha = 0.005$, $B = 1$, $n = 2$, $m = 0.5$				$\alpha = 0.01$, $B = 1$, $n = 4$, $m = 0.75$			
η	R-iter	CG-iter	Max Cond	$\|(\sqrt{k}\|\nabla u\|)\|_p^p$	R-iter	CG-iter	Max Cond	$\|(\sqrt{k}\|\nabla u\|)\|_p^p$
10^3	2	$82, 82$	$1.3e+2$	0.13	1	81	$1.3e+2$	0.13
10^4	2	$85, 85$	$2.5e+2$	0.13	1	84	$2.5e+2$	0.13
10^5	2	$88, 88$	$3.0e+2$	0.13	1	87	$3.0e+2$	0.13
10^6	2	$93, 101$	$3.1e+2$	0.13	1	95	$3.1e+2$	0.13

TABLE 9. Numerical results for preconditioner B_{em}^{-1}. Here we use the van Genuchten model $k(x,u) = k(x)\frac{\{1-(\alpha(|u|/B))^{n-1}[1+(\alpha(|u|/B))^n]^{-m}\}^2}{[1+(\alpha(|u|/B))^n]^{m/2}}$ with k depicted in the left picture of Figure 2. The coarse space dimension is 81.

	$\alpha = 0.005$, $B = 1$, $n = 2$, $m = 0.5$				$\alpha = 0.01$, $B = 1$, $n = 4$, $m = 0.75$			
η	R-iter	CG-iter	Max Cond	$\|(\sqrt{k}\|\nabla u\|)\|_p^p$	R-iter	CG-iter	Max Cond	$\|(\sqrt{k}\|\nabla u\|)\|_p^p$
10^3	2	$76, 76$	$1.6e+2$	0.13	1	88	$1.6e+2$	0.13
10^4	2	$79, 79$	$3.6e+2$	0.13	1	90	$3.6e+2$	0.13
10^5	2	$79, 79$	$4.2e+2$	0.13	1	87	$4.1e+2$	0.13
10^6	2	$80, 81$	$4.2e+2$	0.13	1	90	$4.2e+2$	0.13

TABLE 10. Numerical results for preconditioner B_{em}^{-1}. Here we use the van Genuchten model $k(x,u) = k(x)\frac{\{1-(\alpha(|u|/B))^{n-1}[1+(\alpha(|u|/B))^n]^{-m}\}^2}{[1+(\alpha(|u|/B))^n]^{m/2}}$ with k depicted in the right picture of Figure 2. The coarse space dimension is 81.

	$\alpha = 0.005$, $B = 1$, $n = 2$, $m = 0.5$				$\alpha = 0.01$, $B = 1$, $n = 4$, $m = 0.75$			
η	R-iter	CG-iter	Max Cond	$\|(\sqrt{k}\|\nabla u\|)\|_p^p$	R-iter	CG-iter	Max Cond	$\|(\sqrt{k}\|\nabla u\|)\|_p^p$
10^3	2	33, 33	6.8	0.13	1	33	6.8	0.13
10^4	2	34, 34	6.8	0.13	1	34	6.8	0.13
10^5	2	35, 35	6.8	0.13	1	35	6.8	0.13
10^6	2	36, 36	6.8	0.13	1	36	6.8	0.13

TABLE 11. Numerical results for preconditioner B_{lsm}^{-1}. Here we use the van Genuchten model $k(x,u) = k(x)\frac{\{1-(\alpha(|u|/B))^{n-1}[1+(\alpha(|u|/B))^n]^{-m}\}^2}{[1+(\alpha(|u|/B))^n]^{m/2}}$ with k depicted in the left picture of Figure 2. The coarse space dimension is 166.

	$\alpha = 0.005$, $B = 1$, $n = 2$, $m = 0.5$				$\alpha = 0.01$, $B = 1$, $n = 4$, $m = 0.75$			
η	R-iter	CG-iter	Max Cond	$\|(\sqrt{k}\|\nabla u\|)\|_p^p$	R-iter	CG-iter	Max Cond	$\|(\sqrt{k}\|\nabla u\|)\|_p^p$
10^3	2	32, 32	6.5	0.14	1	31	6.2	0.13
10^4	2	33, 33	6.6	0.13	1	32	6.3	0.13
10^5	2	33, 33	6.6	0.13	1	33	6.3	0.13
10^6	2	35, 35	6.6	0.13	1	34	6.3	0.13

TABLE 12. Numerical results for preconditioner B_{lsm}^{-1}. Here we use the van Genuchten model $k(x,u) = k(x)\frac{\{1-(\alpha(|u|/B))^{n-1}[1+(\alpha(|u|/B))^n]^{-m}\}^2}{[1+(\alpha(|u|/B))^n]^{m/2}}$ with k depicted in the right picture of Figure 2. The coarse space dimension is 184.

$\|\sqrt{k}|\nabla u|\|_p^p, p = 1, 2, 3, \ldots, 10$ is bounded independent of contrast η. We see that the number of outer iterations stays the same for both set of parameters for nonlinearities which means larger α values do not affect the outer iterations. We observe from Tables 13 and 14 (these use different conductivity fields) that the condition numbers in Table 14 are smaller than the corresponding condition numbers in Table 13. This is because conductivity field 2 has simpler subgrid structure compared to conductivity field 1.

Next, we repeat the numerical experiment using the preconditioner B_{em}^{-1} based on the coarse space V_0^{em} and B_{lsm}^{-1} with coarse space V_0^{lsm}. Numerical results for the coarse space B_{em}^{-1} are presented in Tables 15 and 16 while the results for V_0^{lsm} are presented in Tables 17 and 18. As before, we observe that the number of outer iterations is independent of the contrast. However, the for space V_0^{em} the condition number increases as we increase the contrast. On the other hand, the condition number is independent of contrast when V_0^{lsm} is used as a coarse space. Moreover, we observe that the condition number produced by V_0^{lsm}, is only 6 while the condition number for V_0^{em} is about 400 for $\eta = 10^6$. In conclusion, B_{lsm}^{-1} provides a truly independent-of-contrast solver.

5. Conclusions

In this paper, we study robust iterative solvers for finite element discretizations of steady-state Richards' equation. We assume that the nonlinear conductivity field can be written as a product of a nonlinear function and a heterogeneous spatial function that has high contrast. Due to spatial heterogeneities, the number of iterations in an iterative method, in general, will depend on the contrast. To alleviate this problem, we design and investigate iterative solvers that converge independent of the physical parameters (small spatial scales and large contrast). The proposed iterative solvers consist of outer and inner iterations, as it is commonly done in

	$\alpha = 1$, $B = 1$				$\alpha = 2$, $B = 1$			
η	R-iter	CG-iter	Max Cond	$\|(\sqrt{k}\|\nabla u\|)\|_p^p$	R-iter	CG-iter	Max Cond	$\|(\sqrt{k}\|\nabla u\|)\|_p^p$
10^3	4	119, 120	$1.0e+3$	0.13	4	120, 122	$1.1e+3$	0.13
10^4	4	166, 178	$1.1e+4$	0.13	4	173, 181	$1.1e+4$	0.13
10^5	4	224, 224	$1.1e+5$	0.13	4	226, 227	$1.1e+5$	0.13
10^6	4	274, 284	$1.1e+6$	0.13	4	277, 287	$1.1e+6$	0.13

TABLE 13. Numerical results for preconditioner B_{ms}^{-1}. Here we use the Exponential model $k(x,u) = k(x)e^{\alpha(u/B)}$ with k depicted in the left picture of Figure 2. The coarse space dimension is 81.

	$\alpha = 1$, $B = 1$				$\alpha = 2$, $B = 1$			
η	R-iter	CG-iter	Max Cond	$\|(\sqrt{k}\|\nabla u\|)\|_p^p$	R-iter	CG-iter	Max Cond	$\|(\sqrt{k}\|\nabla u\|)\|_p^p$
10^3	4	113, 113	$2.5e+2$	0.13	4	114, 115	$2.5e+2$	0.13
10^4	4	164, 164	$2.5e+3$	0.13	4	164, 164	$2.5e+3$	0.13
10^5	4	223, 232	$2.5e+4$	0.13	4	227, 231	$2.5e+4$	0.13
10^6	4	290, 294	$2.5e+5$	0.13	4	289, 302	$2.5e+5$	0.13

TABLE 14. Numerical results for preconditioner B_{ms}^{-1}. Here we use the Exponential model $k(x,u) = k(x)e^{\alpha(u/B)}$ with k depicted in the right picture of Figure 2. The coarse space dimension is 81.

	$\alpha = 1$, $B = 1$				$\alpha = 2$, $B = 1$			
η	R-iter	CG-iter	Max Cond	$\|(\sqrt{k}\|\nabla u\|)\|_p^p$	R-iter	CG-iter	Max Cond	$\|(\sqrt{k}\|\nabla u\|)\|_p^p$
10^3	3	83, 84	$1.3e+2$	0.13	3	84, 84	$1.3e+2$	0.13
10^4	3	88, 88	$2.5e+2$	0.13	3	89, 90	$2.6e+2$	0.13
10^5	3	90, 91	$3.0e+2$	0.13	3	92, 92	$3.1e+2$	0.13
10^6	3	96, 97	$3.1e+2$	0.13	3	97, 98	$3.1e+2$	0.13

TABLE 15. Numerical results for preconditioner B_{em}^{-1}. Here we use the Exponential model $k(x,u) = k(x)e^{\alpha(u/B)}$ with k depicted in the left picture of Figure 2. The coarse space dimension is 81.

	$\alpha = 1$, $B = 1$				$\alpha = 2$, $B = 1$			
η	R-iter	CG-iter	Max Cond	$\|(\sqrt{k}\|\nabla u\|)\|_p^p$	R-iter	CG-iter	Max Cond	$\|(\sqrt{k}\|\nabla u\|)\|_p^p$
10^3	3	91, 91	$1.6e+2$	0.13	3	91, 92	$1.6e+2$	0.13
10^4	3	95, 95	$3.6e+2$	0.13	3	95, 96	$3.7e+2$	0.13
10^5	3	95, 95	$4.2e+2$	0.13	3	98, 99	$4.2e+2$	0.13
10^6	3	98, 98	$4.2e+2$	0.13	3	99, 99	$4.3e+2$	0.13

TABLE 16. Numerical results for preconditioner B_{em}^{-1}. Here we use the Exponential model $k(x,u) = k(x)e^{\alpha(u/B)}$ with k depicted in the right picture of Figure 2. The coarse space dimension is 81.

the literature. Outer iterations, designed to handle nonlinearities, linearize the equation around the previous solution state. We show that this linearization yields contrast independent iterative

	$\alpha=1$, $B=1$				$\alpha=2$, $B=1$			
η	R-iter	CG-iter	Max Cond	$\|(\sqrt{k}\|\nabla u\|)\|_p^p$	R-iter	CG-iter	Max Cond	$\|(\sqrt{k}\|\nabla u\|)\|_p^p$
10^3	3	33, 33	6.8	0.13	3	34, 34	6.8	0.13
10^4	3	35, 35	6.8	0.13	3	35, 35	6.8	0.13
10^5	3	36, 36	6.8	0.13	3	36, 36	6.9	0.13
10^6	3	37, 37	6.8	0.13	3	37, 37	6.9	0.13

TABLE 17. Numerical results for preconditioner B_{lsm}^{-1}. Here we use the Exponential model $k(x,u)=k(x)e^{\alpha(u/B)}$ with k depicted in the left picture of Figure 2. The coarse space dimension is 166.

	$\alpha=1$, $B=1$				$\alpha=2$, $B=1$			
η	R-iter	CG-iter	Max Cond	$\|(\sqrt{k}\|\nabla u\|)\|_p^p$	R-iter	CG-iter	Max Cond	$\|(\sqrt{k}\|\nabla u\|)\|_p^p$
10^3	3	32, 32	6.4	0.13	3	32, 32	6.6	0.13
10^4	3	34, 34	6.8	0.13	3	34, 34	6.7	0.13
10^5	3	34, 34	6.5	0.13	3	35, 35	6.7	0.13
10^6	3	36, 36	6.8	0.13	3	35, 36	6.7	0.13

TABLE 18. Numerical results for preconditioner B_{lsm}^{-1}. Here we use the Exponential model $k(x,u)=k(x)e^{\alpha(u/B)}$ with k depicted in the right picture of Figure 2. The coarse space dimension is 184.

procedure. For inner iterations, we use recently developed iterative methods (see [15, 17]) that converge independent of the contrast. One of main ingredients of this approach, the construction of coarse spaces, is discussed in details in the paper. Since the same preconditioner was used for every outer iteration, this makes the overall solution process quite efficient. Numerical results are presented to confirm the theoretical findings.

In the future, we would like to study the time-dependent case and the case with non-separable nonlinearities and heterogeneities. In the latter, we plan to develop nonlinear local problems that can identify high-conductivity regions and include these features into the coarse space.

APPENDIX A. PROOF OF THEOREMS 1, 2, AND 3

A.1. **Proof of Theorem 1.** It was shown in [4] that for $\delta>0$ there exists $\epsilon>0$ such that

$$|u_h|_{W_p^1(\Omega)} \leq (1+\delta) \sup_{0\neq v_h\in V^h} \frac{\langle \nabla u_h, \nabla v_h\rangle}{|v_h|_{W_q^1}(\Omega)}, \quad \text{for all } |2-p|\leq \epsilon, \tag{35}$$

where $\frac{1}{p}+\frac{1}{q}=1$ and δ and ϵ are independent of h. Now, we consider a high-contrast case via a perturbation argument.

Define a bilinear form $\mathcal{B}: W_p^1(\Omega)\times W_q^1(\Omega)\to\mathbb{R}$ by

$$\mathcal{B}(u,v) \;:=\; \langle \nabla u, \nabla v\rangle - \frac{1}{M} a(u,v;\cdot).$$

It follows from Assumption 1 (A) and Hölder's inequality that

$$\mathcal{B}(u,v) \leq \left(1-\frac{C_0}{M}\right)\int_\Omega |\nabla u(x)\nabla v(x)|dx \leq \left(1-\frac{C_0}{M}\right)|u|_{W_p^1(\Omega)}|v|_{W_q^1(\Omega)}. \tag{36}$$

Note that $C_0/M < 1$. Then, the identity $\langle \nabla u, \nabla v\rangle = \mathcal{B}(u,v) + \frac{1}{M}a(u,v;\cdot)$, together with estimates (35) and (36) yields

$$M\left(\frac{1}{1+\delta} - \left(1 - \frac{C_0}{M}\right)\right)|u_h|_{W_p^1(\Omega)} \leq \sup_{0\neq v_h\in V^h} \frac{a(u_h, v_h;\cdot)}{|v_h|_{W_q^1(\Omega)}}.$$

Let $\delta = \frac{C_0}{2M-C_0}$, and choose ϵ to be as given in (35) for this particular choice of δ. Then, $M\left(\frac{1}{1+\delta} - \left(1-\frac{C_0}{M}\right)\right) = C_0/2$. Recall that $a(u,v;\cdot)$ can be very large because of high contrast. This completes the proof. Note that ϵ and α depend only on the constants C_0, C^* and M, though the coercivity bound is independent of the contrast M. □

A.2. **Proof of Theorem 2.** (a) For any $u_h \in V_h^{\mathcal{K},p}$, $k(x)\lambda(x,u_h)$ satisfies the conditions of Theorem 1 with a constant M_0 such that

$$M_0 = \sup\{k(x)\lambda(x,s) : \|s\|_{L^\infty} \leq c_p|\log h|\mathcal{K}\}, \tag{37}$$

where h is the mesh-size of the partition $\mathcal{T}_h$ and c_p is the constant in Sobolev's inequality [4],

$$\|v\|_{L^\infty(\Omega)} \leq c_p|\log h|\|v\|_{W_p^1(\Omega)}, \quad \text{for all } v \in W_p^1(\Omega). \tag{38}$$

The constant M_0 exists because of Assumption 1 (A) and (B). Then, $u_h \in V_h^{\mathcal{K},p}$ implies that $\|u_h\|_{L^\infty(\Omega)} \leq c_p|\log h|\|u_h\|_{W_p^1(\Omega)} \leq c_p|\log h|\mathcal{K}$ and hence $\sup\{k(x)\lambda(x,u_h)\} \leq M_0$. For sufficiently small $\mathcal{K}$ (e.g., $\mathcal{K} = C/c_p$) there is a $p > 2$ such that the inequality (29) in Theorem 1 holds. Then,

$$\begin{aligned}
\|T_h u_h\|_{W_p^1(\Omega)} \leq &\quad \alpha \sup_{0\neq v_h\in V^h} \frac{a(T_h u_h, v_h; u_h)}{|v_h|_{W_q^1(\Omega)}} && \text{(from Theorem 1)}\\
= &\quad \alpha \sup_{0\neq v_h\in V^h} \frac{F(v_h)}{|v_h|_{W_q^1(\Omega)}} \leq \quad C\|F\|_{W_p^{-1}(\Omega)}.
\end{aligned}$$

Choose $\|F\|_{W_p^{-1}(\Omega)} \leq \mathcal{K}/C$ to get $\|T_h u_h\|_{W_p^1(\Omega)} \leq \mathcal{K}$, i.e., T_h maps $V_h^{\mathcal{K},p}$ into itself. By Browder fixed point [11], there exists a solution $\tilde{u}_h$ of equation (7) and it satisfies

$$T_h\tilde{u}_h = \tilde{u}_h. \tag{39}$$

□

(b) Now, we shall show the mapping T_h is contraction and also that the contractivity constant is independent of the contrast.

Suppose $u_h, v_h \in V_h^{\mathcal{K},p}$ satisfy $a(T_h u_h, w; u_h) = F(w)$ and $a(T_h v_h, w; v_h) = F(w)$. Thus,

$$a(T_h u_h, w; u_h) - a(T_h v_h, w; v_h) \quad = \quad 0. \tag{40}$$

Since $a(\cdot,\cdot,\cdot)$ is a bilinear form, from equation (40) we get

$$a(T_h u_h - T_h v_h, w; u_h) \quad = \quad a(T_h v_h, w; v_h) - a(T_h v_h, w; u_h). \tag{41}$$

Now, using the definition of $a(\cdot,\cdot,\cdot)$, the right hand side of the equation (41) can be written as

$$
\begin{aligned}
&\int_\Omega k(x)(\lambda(x,v_h)-\lambda(x,u_h))\nabla T_h v_h \nabla w dx \\
&\quad\le \left(\int_\Omega k(x)(\nabla T_h v_h)^2 |\lambda(x,v_h)-\lambda(x,u_h)|^2 dx\right)^{\frac{1}{2}} \left(\int_\Omega k(x)(\nabla w)^2 dx\right)^{\frac{1}{2}} \\
&\quad\le \left(\int_\Omega |k(x)|^q |\nabla T_h v_h|^{2q} dx\right)^{\frac{1}{2q}} \left(\int_\Omega |\lambda(x,v_h)-\lambda(x,u_h)|^{2q'} dx\right)^{\frac{1}{2q'}} \\
&\qquad \cdot \left(\int_\Omega k(x)(\nabla w)^2 dx\right)^{\frac{1}{2}} \text{ (By Hőlder's inequality, } \frac{1}{q}+\frac{1}{q'}=1) \\
&\quad\le \left(\int_\Omega |k(x)|^q |\nabla T_h v_h|^{2q} dx\right)^{\frac{1}{2q}} \left(C_1 \int_\Omega |v_h-u_h|^{2q'} dx\right)^{\frac{1}{2q'}} \\
&\qquad \cdot \left(\int_\Omega k(x)(\nabla w)^2 dx\right)^{\frac{1}{2}} \qquad \text{(By Lipschitz continuity of } \lambda) \\
&\quad\le \left(\int_\Omega |k(x)|^q |\nabla T_h v_h|^{2q} dx\right)^{\frac{1}{2q}} \left(C_1 C_{2q'} \int_\Omega (\nabla(v_h-u_h))^2 dx\right)^{\frac{1}{2}} \\
&\qquad \cdot \left(\int_\Omega k(x)(\nabla w)^2 dx\right)^{\frac{1}{2}}, \text{ (by Sobolev inequality),}
\end{aligned}
\tag{42}
$$

where we have used the Sobolev inequality $\|u\|_{L^{2q'}(\Omega)} \le C_{2q'}\|Du\|_{L^2(\Omega)}$ with $2q' \in [1,\infty]$ for function u with bounded mean oscillation. Next, we want to bound $\left(\int_\Omega |k(x)|^q |\nabla T_h v_h|^{2q} dx\right)^{\frac{1}{2q}}$ with some constant which is independent of the contrast, i.e., the constant doesn't depend on $k(\cdot)$.

Now, we make the following assumption, which is slightly different than Assumption 1(C).

Assumption 2. *Given the equation $a(T_h v_h, T_h v_h, v_h) = F(T_h v_h)$ (see (8)), we assume that*

$$
\int_\Omega (k(x)|\nabla T_h v_h|^2)^{q/2} dx \le C_F^q, \tag{43}
$$

where $C_F^q \to 0$ as $\|F\|_{W_q^{-1}(\Omega)} \to 0$ for some $q > 2$.

We note that when $F = 0$ then $C_F^2 = 0$, thus, $T_h v_h$ is zero almost everywhere. Moreover, if $\|F\|_{W_2^{-1}(\Omega)}$ is small, then C_F^2 is small and C_F^2 converges to zero as $\|F\|_{W_2^{-1}(\Omega)}$ goes to zero. The inequality (43) assumes that we have continuity of C_F^q with respect to $\|F\|_{W_2^{-1}(\Omega)}$ for any $q > 2$ that is sufficiently close to 2. We note that $\|T_h v_h\|_{W_q^1(\Omega)}$ is bounded by $\|F\|_{W_q^{-1}(\Omega)}$ as shown above. This is typically used to show the contractivity of the map T_h.

Now, we can conclude that

$$
\begin{aligned}
&\int_\Omega k(x)(\lambda(x,v_h)-\lambda(x,u_h))\nabla T_h v_h \nabla w dx \\
&\qquad\qquad \le C \left(\int_\Omega (\nabla(v_h-u_h))^2 dx\right)^{\frac{1}{2}} \left(\int_\Omega k(x)(\nabla w)^2 dx\right)^{\frac{1}{2}},
\end{aligned}
\tag{44}
$$

where the constant C depends on Lipschitz constant C_1.

Now put $w = T_h u_h - T_h v_h$, then left hand side of (41) is bounded below,

$$\begin{aligned} a(T_h u_h - T_h v_h, T_h u_h - T_h v_h, u_h) &= \int_\Omega (k(x)\lambda(x,u_h)(\nabla(T_h u_h - T_h v_h))^2 dx \\ &\geq C_2 \int_\Omega k(x)(\nabla(T_h u_h - T_h v_h))^2 dx. \end{aligned} \tag{45}$$

Combine equations (44) and (45), then we get

$$\int_\Omega k(x)(\nabla(T_h u_h - T_h v_h))^2 dx \leq C_2^{-1} C \left(\int_\Omega (\nabla(v_h - u_h))^2 dx\right)^{\frac{1}{2}} \left(\int_\Omega k(x)(\nabla(T_h u_h - T_h v_h))^2 dx\right)^{\frac{1}{2}}.$$

Then, using the Assumption 1 (a), we get

$$C_0^{\frac{1}{2}} \left(\int_\Omega (\nabla(T_h u_h - T_h v_h)^2 dx\right)^{\frac{1}{2}} \quad \leq \quad C_2^{-1} C \left(\int_\Omega (\nabla(v_h - u_h))^2 dx\right)^{\frac{1}{2}}.$$

So we can deduce that

$$|T_h u_h - T_h v_h|_{W_2^1} \leq C_0^{-\frac{1}{2}} C_2^{-1} C |u_h - v_h|_{W_2^1}, \tag{46}$$

i.e., the mapping T_h is a contraction if C is chosen sufficiently small (see Assumption 2).

A.3. **Proof of Theorem 3.** From Lemma 1 and Lemma 10 of [17] we have that there is a *stable decomposition*, that is, there exists $v_0 \in V_0^{lsm}$, $v_i \in V_0^h(\omega_i)$, $i = 1, \ldots, N_v$, such that

$$\int_D k|\nabla v_0| + \sum_{i=1}^{N_v} \int_{\omega_i} k|\nabla v_i|^2 \leq C_0 \left(1 + \frac{1}{H^2 \mu_{L+1}}\right) \int_D k|\nabla v|^2,$$

for some positive constant independent of the contrast and $\mu_{L+1} = \min_i \mu_{L_i+1}$. Here we select the first L_i smallest eigenvalues of (24). Then, for a fixed w we have stable decomposition,

$$\begin{aligned} &\int_D \lambda(x,w)k(x)|\nabla v_0(x)| + \sum_{i=1}^{N_v} \int_{\omega_i} \lambda(x,w)k(x)|\nabla v_i|^2 \\ &\qquad \leq \quad C_0 \frac{\max_{x\in D} \lambda(x,w)}{\min_{x\in D} \lambda(x,\omega)} \left(1 + \frac{1}{H^2 \mu_{L+1}}\right) \int_D \lambda(x,w)k(x)|\nabla v|^2. \end{aligned}$$

According to the abstract theory of domain decomposition, see [32, 25], we conclude that the condition number of the preconditioned matrix is of order

$$cond(B^{-1}A) \leq C_0 \frac{\max_{x\in D} \lambda(x,w)}{\min_{x\in D} \lambda(x,\omega)} \left(1 + \frac{1}{H^2 \mu_{L+1}}\right).$$

Further noting that the number of nonlinear outer iterations is bounded (see Theorem 2), we conclude that the proposed iterative procedure converges independent of the contrast.

Acknowledgments

The research of Y. Efendiev, J. Galvis, and R. Lazarov has been supported in parts by award KUS-C1-016-04, made by King Abdullah University of Science and Technology (KAUST). S. Ki Kang and R. Lazarov are also supported in part by the award made by NSF DMS-1016525. S.K. Kang is grateful to Fraunhofer Institute for Industrial Mathematics (ITWM) for hosting her visit in the Spring 2011.

References

[1] A. Abdulle and G. Vilmart, *A priori error estimates for finite element methods with numerical quadrature for nonmonotone non linear elliptic problems*, Submitted for publication.

[2] J. Aarnes and T. Hou, *Multiscale domain decomposition methods for elliptic problems with high aspect ratios*, Acta Math. Appl. Sin. Engl. Ser., 18(1), 2002, pp. 63-76.

[3] J. Bergh and J. Löfstrom, *Interpolation Spaces, an Introduction*, Springer-Verlag, Berlin, 1976.

[4] S.C. Brenner and L.R. Scott, *The Mathemethical Theory of Finite Element Methods*, Springer-Verlag, 1994.

[5] X.C. Cai and D.E. Keyes, *Nonlinearly preconditioned inexact Newton algorithms*, SIAM J. Sci. Comput., 24, 2002, pp. 183-200.

[6] X.C. Cai, L. Marcinkowski, and P. Vassilevski, *An element agglomeration nonlinear additive Schwarz preconditioned Newton method for unstructured finite element problems*, Appl. Math., 50, no. 3,2005, pp. 247275.

[7] G. Chavent and J. Jaffré, *Mathematical Models and Finite Elements for Reservoir Simulation; Single Phase, Multiphase and Multicomponent Flows through Porous Media*, Elsevier Science Publishers, North-Holland, Amsterdam, New York, Oxford, Tokyo, 1986.

[8] Z. Chen, W.B. Deng, and H. Ye, *Upscaling of a class of nonlinear parabolic equations for the flow transport in heterogeneous porous media*, Communications in Mathematical Sciences 3 (2005), 493-515.

[9] P.G. Ciarlet, *The Finite Element Method for Elliptic Problems*, North-Holland, Amsterdam, New York, Oxford, 1988.

[10] M. Dryja and W. Hackbusch, *On the nonlinear domain decomposition method*, BIT Numerical Mathematics, Volume 37, Number 2, pp. 296-311, DOI: 10.1007/BF02510214

[11] J. Dugundgi, *Topology*, Allyn and Bacon, Boston, 1966

[12] Y. Efendiev and T. Hou, *Multiscale finite element methods. Theory and applications*, Springer, 2009.

[13] Y. Efendiev, T. Hou and V. Ginting, *Multiscale finite element methods for nonlinear partial differential equations*, Comm. Math. Sci., 2(4), 2004

[14] Y. Efendiev, T.Y. Hou, and X.H. Wu, *Convergence of a nonconforming multiscale finite element method*, SIAM J. Num. Anal., 37 2000, pp. 888-910.

[15] Y. Efendiev and J. Galvis, *Domain decomposition preconditioner for multiscale high-contrast problems*, in: Y. Huang, R. Kornhuber, O. Widlund, J. Xu (Eds.), Domain Decomposition Methods in Science and Engineering XIX, Volume 78 of Lecture Notes in Computational Science and Engineering, Springer-Verlag, Berlin, 2011, pp. 189-196.

[16] Y. Efendiev, J. Galvis, and P. Vassielvski, *Spectral Element Agglomerate Algebraic Multigrid Methods for Elliptic Problems with High-Contrast Coefficients*, in Domain Decomposition Methods in Science and Engineering XIX, Huang, Y.; Kornhuber, R.; Widlund, O.; Xu, J. (Eds.), Volume 78 of Lecture Notes in Computational Science and Engineering, Springer-Verlag, 2011, Part 3, pp. 407-414.

[17] J. Galvis, and Y. Efendiev, *Domain decomposition preconditioners for multiscale flows in high contrast media*, Multiscale Model. Simul. 8, 2010, pp. 1461-1483.

[18] J. Galvis, and Y. Efendiev, *Domain decomposition preconditioners for multiscale flows in high contrast media. Reduced dimension coarse spaces*, Multiscale Model. Simul. 8, 2010, pp. 1621-1644.

[19] I.G. Graham, P.O. Lechner, and R. Scheichl, *Domain decomposition for multiscale PDEs*, Numer. Math., 106(4), 2007, pp. 589-626.

[20] I.G. Graham and R. Scheichl, *Robust domain decomposition algorithms for multiscale PDEs*, Numer. Methods Partial Differential Equations, 23(4), 2007, pp. 859-878.

[21] R. Haverkamp, M. Vauclin, J. Touma, P. Weirenga, and G. Vachaud, *Comparison of numerical simulation models for one-dimensional infiltration*, Soil Sci. Soc. Am. J., 41, 1977, pp. 285-294.

[22] T.Y. Hou and X.H. Wu, *A multiscale finite element method for elliptic problems in composite materials and porous media*, Journal of Computational Physics, 134, 1997, pp.169-189.

[23] P. Jenny, S.H. Lee, and H. Tchelepi, *Multi-scale finite volume method for elliptic problems in subsurface flow simulation*, J. Comput. Phys., 187, 2003, pp. 47-67.

[24] T. Kim, J. Pasciak, and P. Vassilevski, *Mesh-independent convergence of the modified inexact Newton method for a second order non-linear problem*, Numer. Linear Algebra Appl., 13,no. 1, 2006, pp. 2347.

[25] T.P.A. Mathew, *Domain decomposition methods for the numerical solution of partial differential equations*, volume 61 of Lecture Notes in Computational Science and Engineering, Springer-Verlag, Berlin, 2008.

[26] N.G. Meyers, *An L^p-estimate for the gradient of solutions of second order elliptic divergence equations*, Annali dela Scuola Normale Superiore di Pisa, Ser. III, XVII, 1963, pp. 189-206.

[27] S.K. Rajagopal, *On a hierarchy of approximate models for flows in incompressible fluids through porous solids*, Math. Models Methods Appl. Sci., 17, 2007, pp.215-252.

[28] L. Richards, *Capillary conduction of liquids through porous mediums*, Physics, 1931, pp. 318-333.
[29] A.J. Salgado, *Approximation techniques for incompressible flows with heterogeneous properties*, PhD. Thesis, Texas A&M University, 2010.
[30] C.G. Simader, *On Dirichlet's Boundary Value Problem*, Lecture Notes in three dimensions. Numer.Math.60, 1991, pp. 219-234.
[31] X.C. Tai and M. Espedal, *Applications of a space decomposition method to linear and nonlinear elliptic problems*, Numer. Methods Partial Differential Equations 14, no. 6,1998, pp. 717737.
[32] A. Toselli and O. Widlund. *Domain decomposition methods—algorithms and theory*, volume 34 of Springer Series in Computational Mathematics, Springer-Verlag, Berlin, 2005.
[33] M.Th. vanGenuchten, *A closed form equations for predicting the hydraulic conductivity of unsaturated soils*, Soil Sci. Soc. Am. J., 44, 1980, pp. 892-898.
[34] J. Xu, *Two-grid discretization techniques for linear and nonlinear PDEs*, SIAM Journal on Numerical Analysis 33, 1996, pp.1759-1777
[35] J. Xu and L. Zikatanov. *On an energy minimizing basis for algebraic multigrid methods*. Comput. Visual. Sci., 7, 2004, pp.121-127.

Department Mathematics, TAMU, College Station, Texas, 77843, USA (efendiev@math.tamu.edu)

Department of Mathematics, TAMU, College Station, Texas, 77843, USA, (jugal@math.tamu.edu)

Department of Mathematics, TAMU, College Station, Texas, 77843, USA (kang@math.tamu.edu)

Department of Mathematics, TAMU, College Station, Texas, 77843, USA (lazarov@math.tamu.edu)